Hindawi
Geofluids
Volume 2023, Article ID 2916702, 15 pages
https://doi.org/10.1155/2023/2916702

Research Article

Dynamic Pressure Manifestation Mechanism and Control Techniques for Roadways with Large Mining Heights and Intense Mining: A Case Study

Dong Xu,[1,2] **Mingshi Gao**,[1,2] **and Xin Yu**[1,2]

[1]*School of Mines, Key Laboratory of Deep Coal Resource Mining, China University of Mining and Technology, Xuzhou, Jiangsu 221116, China*
[2]*The State Key Laboratory of Coal Resources and Safe Mining, China University of Mining and Technology, Xuzhou, Jiangsu 221116, China*

Correspondence should be addressed to Mingshi Gao; cumt_gms@cumt.edu.cn

Received 8 October 2022; Revised 6 November 2022; Accepted 3 April 2023; Published 17 April 2023

Academic Editor: Jinpeng Zhang

Copyright © 2023 Dong Xu et al. This is an open access article distributed under the Creative Commons Attribution License, which permits unrestricted use, distribution, and reproduction in any medium, provided the original work is properly cited.

Responding to severe surrounding rock deformation failures and other problems in roadways in western China with large mining heights and intense mining, the work presented in this paper studied the mechanism of surrounding rock deformation failures in roadways with dynamic pressure through field investigations, theoretical analysis, and numerical simulation. According to the research findings, mining roadway deformation failures are affected by roadway layout orientation, working face mining intensity, and dynamic load disturbances from roof breakage. Coal pillars, as bridges connecting the roof and floor, constitute the energy transfer path near roadways surrounding rock, and an unreasonable coal pillar size and lateral overhanging roof structure may aggravate static load energy accumulation in the roadway surrounding rock. Roadway protection with small or large coal pillars may increase elastic energy loss in the energy transfer path; a reasonable size of small and large coal pillars is 15 m and 35 m, respectively. Using roof cutting for pressure relief may reduce the elastic energy of roadway surrounding rock by 14.35-26.33% during primary mining and 21.57-29.31% during secondary mining, thereby reducing the static load elastic energy in the surrounding rock and improving the stability of roadway surrounding rock.

1. Introduction

Since roadways are a key component of the production and transportation system in coal mines, improving their safety, reliability, and stability is of great importance for coal mine production. With the recent increase in coal mining depths and intensity; however, dynamic pressure phenomena such as rib spalling, floor heave, and roof fall have appeared frequently in roadway surrounding rock, posing serious threats to safety and efficient production [1–4]. In response, many scholars have intensively studied the dynamic pressure manifestation in coal mine roadways. Lai et al. [5] reported that the absence of support at roadway floors and mining disturbances causes extruded flowing floor heave. Zhai et al. [6] studied the floor heave mechanism in water-rich soft rock roadways and built an asymmetric floor heave mechanical model. Chen et al. [7] proposed the "pressure relief-support" control scheme to solve the floor heave problem in the Zaoquan Coal Mine. Through experiments, Sun et al. [8] found that horizontal stress has a great impact on the floor heave of roadways and that rock mass failure is often accompanied by abnormal temperature changes. Mo et al. [9, 10] studied the floor buckling failure mechanism by classifying roadway floors. Peng et al. [11] analysed the failure mechanism of rock with high horizontal stresses surrounding roadways and proposed the multistage support control technique. Xiong et al. [12] studied the cyclic failure mechanism of inclined roadways and revealed the principle of roadway deformation control. Through a study on the large deformation mechanism in soft rock roadways, Liu et al. [13] analysed the failure sequence of the surrounding rock and proposed the zoned coupling support technique. Li et al. [14] studied the rib spalling mechanism

in deep soft coal roadways and analysed the relationship between coal wall spalling and the mechanical properties of the coal and the rock. Zhang et al. [15] built a mechanical model of roof breakage at the end of the working face, analysed the deflection distribution characteristics of thin plates with different length-to-width ratios, and revealed the end roof fall failure mechanism. Wang et al. [16] studied the spatiotemporal evolution law of stresses and cracks in the rock surrounding deep-buried inclined jointed rock roadways and revealed the asymmetric deformation failure mechanism of the rock surrounding deep roadways. Shen and Barton [17] worked with fracture mechanics to study the rib spalling failure mechanism in roadways and simulated the law of crack initiation and propagation using FRACOD codes. Feng et al. [18] used simulation software to analyse the effects of the magnitude and direction of the principal stress on the plastic zones of mining roadways and revealed the surrounding rock deformation failure mechanism. Wang et al. [19] found that high tectonic stresses and fault slips resulting from mining activities are the top cause of roadway deformation and roof falls in geologically complex areas. Jiang et al. [20] studied the roof-caving failure mechanism in the water-rich rock surrounding roadways based on plastic mechanics by analysing the law of effects of the various mechanical parameters on roof failure. Dong et al. [21] studied the distribution characteristics of the surrounding rock fracture zone in mining roadways with composite roofs and constrained the large deformations in the rock surrounding roadways through the combined "bolt + anchor cable + metal mesh" support technique. Kang et al. [22] built a mechanical model of sliding floor heave and determined the relation between the critical damage depth of roadway floors and the minimum support depths. Cao et al. [23] explored the floor extrusion failure mechanism in deep roadways with high horizontal stresses and presented a support strategy to prevent the plastic slip of a roadway floor. Yan et al. and Zhu et al. [24, 25] studied the roof-caving mechanism of roadways with extrathick coal seams and revealed that the joint fissure development of coal seams and the influence of mining were the main causes of roadway roof failure. Xu et al. [26] found that uneven stress in a roadway led to asymmetric deformation of the surrounding rock, which induced roof caving.

Since the coal seams in western China feature shallow burial depths, large thicknesses, and high mining intensities, double roadway excavation driving is generally used. The roadways are affected by driving and primary and secondary mining, which cause intense dynamic load disturbances and severe surrounding rock deformation failures. However, few studies have been conducted on the dynamic pressure manifestation mechanism in the rock surrounding shallow roadways with large mining heights and intense mining. Therefore, the work presented in this paper analysed the dynamic pressure manifestation mechanism in the roadway surrounding rock by exploring the evolution law of the surrounding rock energy during roadway driving and mining in a mine in Shaanxi Province after having proposed restrictions on the surrounding rock deformations by optimizing coal pillar sizes and roof-cutting procedures for pressure relief, thereby providing technical support for the management of similar roadways in western China.

2. Engineering Background

2.1. Engineering Overview. The studied mine is situated in Yulin, Shaanxi Province, where coal seam #2 is currently under mining. The average burial depth of the working face is 321.6 m, the average thickness of the coal seam is 6 m, the dip length of the working face is 350 m, and the strike length is 4000-6000 m. The working face was designed with two roadways, one of which will be preserved as the return air roadway for the next working face. The widths of the roadway section and segment coal pillars are 25.08-27.95 m^2 and 20 m, respectively. The mining speed of the working face is 15-20 m/d, and the mining roadways of the mine are typical shallow roadways with large mining heights and intense mining. The layout of the roadway and working face is shown in Figure 1. The roadways have developed severe floor heave, rib spalling, and end roof falls during working face mining. The floor heaves have reached 0.5-1.2 m in size, and the maximum size of a falling block has reached 15 m^3. These conditions have a strong impact on mine safety and production efficiency.

2.2. Analysis of the Causes of Roadway Failure. Roadway surrounding rock failures are primarily caused by the roadway layout orientation, the mining intensity, and the dynamic load disturbances of the roof Figure 2.

(1) *Irrational roadway layout orientation*. The maximum and minimum horizontal principal stresses of the roadway surrounding rock are 16.62 and 8.68 MPa, respectively, and the axial angle between the maximum horizontal principal stress and the mining roadway is 80°, i.e., approximately perpendicular to the mining roadway. Since the mining roadway is in the most disadvantageous stressing position, the stability of the roadway surrounding rock is poor

(2) *High mining intensity on the working face*. The working face is characterized by a large coal seam mining height, a long dip, a long strike distance, and a high daily mining rate. In addition, the roadway surrounding rock is subjected to the impact of driving and primary and secondary mining, leading to a long maintenance cycle for the roadway. Thus, roadways are difficult to maintain because of the high mining intensity

(3) *Intensive dynamic load disturbance on the mining roadway*. Multiple layers of hard sandstone roofs in the overlying strata above the working face have thicknesses of more than 10 m. Hard roof breakage may easily result in an overhanging structure, and high static load-concentrated stresses can be generated in the roadway surrounding rock. The superposition of these effects combined with the periodic fracture of other overlying sandstone layers leads to intensive dynamic load disturbances in the roadway surrounding rock

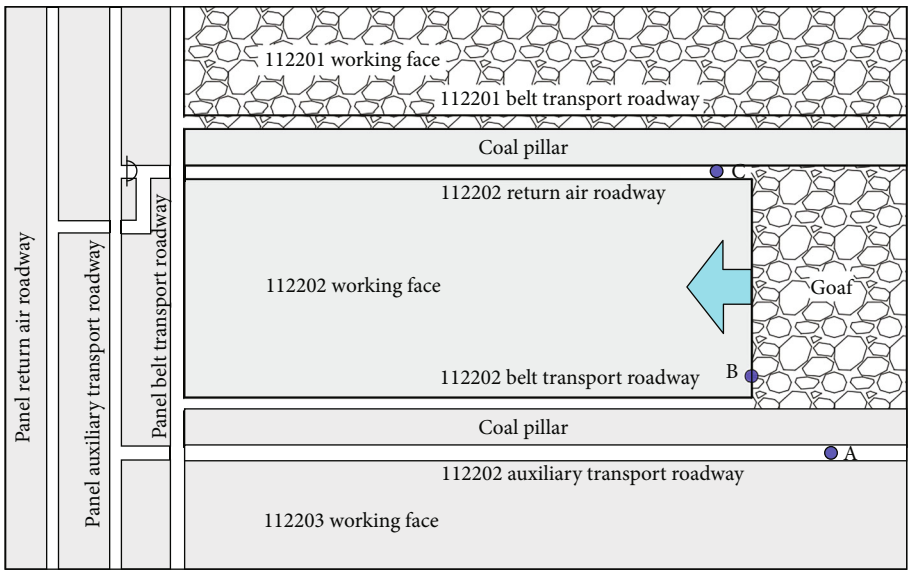

Figure 1: Location diagram of the roadway and working face.

Figure 2: Roadway deformation and failure diagram.

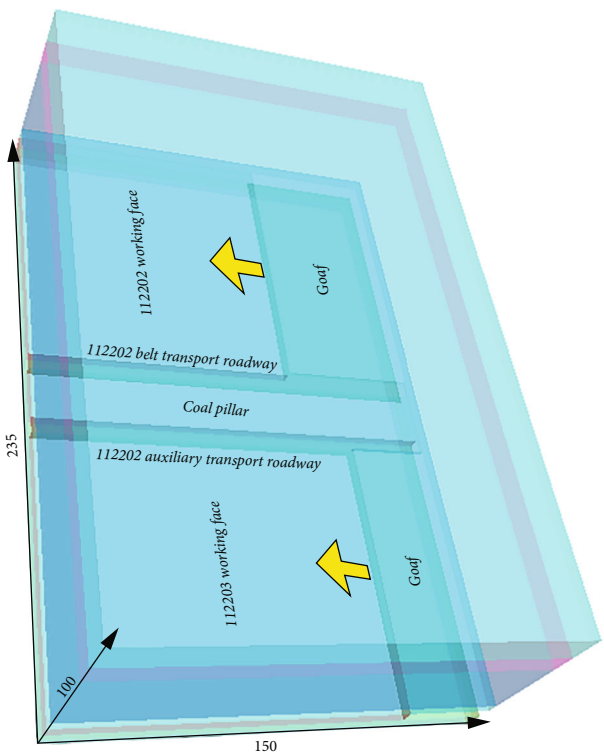

Figure 3: Numerical model.

3. Mechanism of the Dynamic Pressure Manifestation in the Roadway Surrounding Rock with Large Mining Heights and Intense Mining

3.1. Simulation of the Dynamic Pressure Manifestation in the Roadway Surrounding Rock. To study the mechanism of the dynamic pressure manifestation in the roadway surrounding rock with large mining heights and intense mining, a 235 × 150 × 100 m three-dimensional model was built with FLAC3D numerical software based on the geological conditions of working faces 112202 and 112203. The numerical calculation model is shown in Figure 3. The physical and mechanical parameters of various rock masses are listed in Table 1. The Mohr-Coulomb criterion was applied to the model in which the roof must bear a load of 5.8 MPa, and the lateral and floor boundaries are fixed and constrained. According to the actual mining situation, the excavation sequence of the model is given as follows: auxiliary and belt transport roadway 112202 → working face 112202 → working face 112203. The energy evolution characteristics of the roadway surrounding rock at different stages of driving and mining were simulated to analyse the roadway dynamic pressure manifestation process. The rock stratum histogram in the working face is shown in Figure 4.

As shown in Figure 5, an energy release zone is formed near the surrounding rock due to the unloading effect during the double roadway excavation driving, which reduces the elastic energy in the coal pillars and floor; the bending subsidence deformation causes the accumulated elastic energy in the roadway roof to increase slightly to 2.44×10^4 J. Overall, the comparative analysis indicates that the stress disturbance in the surrounding rock is not substantial, and the roadway is highly stable.

Table 1: Mechanical parameters of various rock masses of the numerical model.

Lithology	ρ (kg/m^3)	E (GPa)	c (MPa)	θ (°)	σ_t (MPa)
Mudstone	2465	6.16	1.21	23.25	0.61
Fine sandstone	2834	18.9	3.2	35.49	1.31
Siltstone	2460	19.1	3.75	36.52	1.84
Medium sandstone	2280	24.03	2.26	35.41	1.22
Coal	1320	9.51	0.61	38.48	0.51

As shown in Figure 6, the stoping operation in the simulation is performed at working face 112202, and the gateway for belt and auxiliary transport at 112202 is affected by primary mining. Thus, O-X breakage develops at the goaf roof of the working face; the side roof of belt transport roadway 112202 turns into a curved triangular plate, through which the rotary subsidence leads to static load energy agglomeration at the side of the coal pillars against the goaf, where the energy reaches 5.81×10^5 J. The energy in the coal pillars against auxiliary transport roadway 112202 reaches 4.49×10^5 J, while the intermediate energy of the coal pillars is 2.88×10^5 J. The energy inside the coal pillars is distributed in an asymmetrical saddle shape as a whole, and the peak energy on both sides is located at 3.1 m inside the coal pillars of the roadway. The overburden roof transfers force through the coal pillars, and the mudstone elastic energy in the floor of the coal pillars reaches 5.62×10^5 J; high static load energy agglomeration comes into being near the coal pillars behind the goaf, while the goaf-side segment of auxiliary transport roadway 112202 is a free space, where the elastic energy is zero; thus, an energy transfer path develops in the roadway surrounding rock, and the elastic energy in the coal pillars and floor results in rib spalling and floor heave along the empty roadway. Due to roof convergence, static load energy agglomeration develops inside the coal mass in the end area of working face 112202, and the energy reaches 4.22×10^5 J. Meanwhile, the floor stratum elastic energy in the coal pillars behind the goaf can still be transferred to the leading segment of the working face, and thus, rib spalling and floor heave may frequently appear in the leading working face area of belt transport roadway 112202. Furthermore, static load energy agglomeration develops in the roof within 20 m from working face end 112202 to the gateway, and the energy reaches 4.25×10^5 J; thus, the end area of the working face is prone to experiencing roof fall due to the dynamic load of periodic breakage in the overburden.

During the stoping operation at working face 112203, auxiliary transport roadway 112202 serves as a preserved roadway and turns into the return air gateway for working face 112203; then, return air roadway 112203 undergoes

Thickness (m)	Histogram	Lithology	Lithology description
14.9		Fine sandstone	Greyish white, mainly composed of quartz
10.7		Siltstone	Grey, wavy bedding, with thin mudstone layer in the rock stratum
35.3		Medium sandstone	Grey white, mainly composed of quartz feldspar, massive bedding, hard and dense rock core
4.9		Fine sandstone	Greyish white, mainly composed of quartz
6.1		Coal	Bright coal, the gangue in the coal seam is medium sandstone
12.5		Mudstone	Dark grey, wavy bedding, with sliding surface
14.3		Fine sandstone	Greyish white, mainly composed of quartz

Figure 4: Rock stratum histogram.

secondary mining. Figure 7 shows that with the advance of the face, the energy distribution of the coal pillar behind the goaf at working face 112203 is still saddle-shaped, and the energy in the coal pillar at the goaf side at 112202 reaches 8.69×10^5 J, while the energy in the coal pillar at the goaf side at 112203 reaches 7.95×10^5 J. The intermediate energy of the coal pillars reaches 5.21×10^5 J, that is, the static load energy agglomeration in the coal pillar increases by 49.57-80.90% compared with that of the primary mining. The energy is distributed asymmetrically in the coal pillar, indicating that lateral overhang still exists; the high static load energy is transferred forwards via the elastic kernel in the coal pillars to worsen the rib spalling in the coal pillars at the leading segment of the return air roadway. Moreover, due to the enhanced impact of secondary mining, the accumulated elastic energy in the coal pillar floor mudstone reaches 9.19×10^5 J, an increase by 63.52% compared with that of primary mining. The high static load energy is transferred to the front of the working face, worsening the floor heave in the leading segment of the return air roadway. The static load energy agglomeration develops inside the coal mass in the end area of the return air roadway and reaches 5.77×10^5 J, an increase by 52.65% compared with that of primary mining; accordingly, the rib spalling in the stoping operation at the return air roadway worsens.

Overall, the comparative analysis indicates that the coal pillars do not completely undergo plastic yield failure after driving and primary and secondary mining, and an elastic kernel with a certain width remains in the middle of the coal pillars. Under the action of the lateral overhang in the goaf,

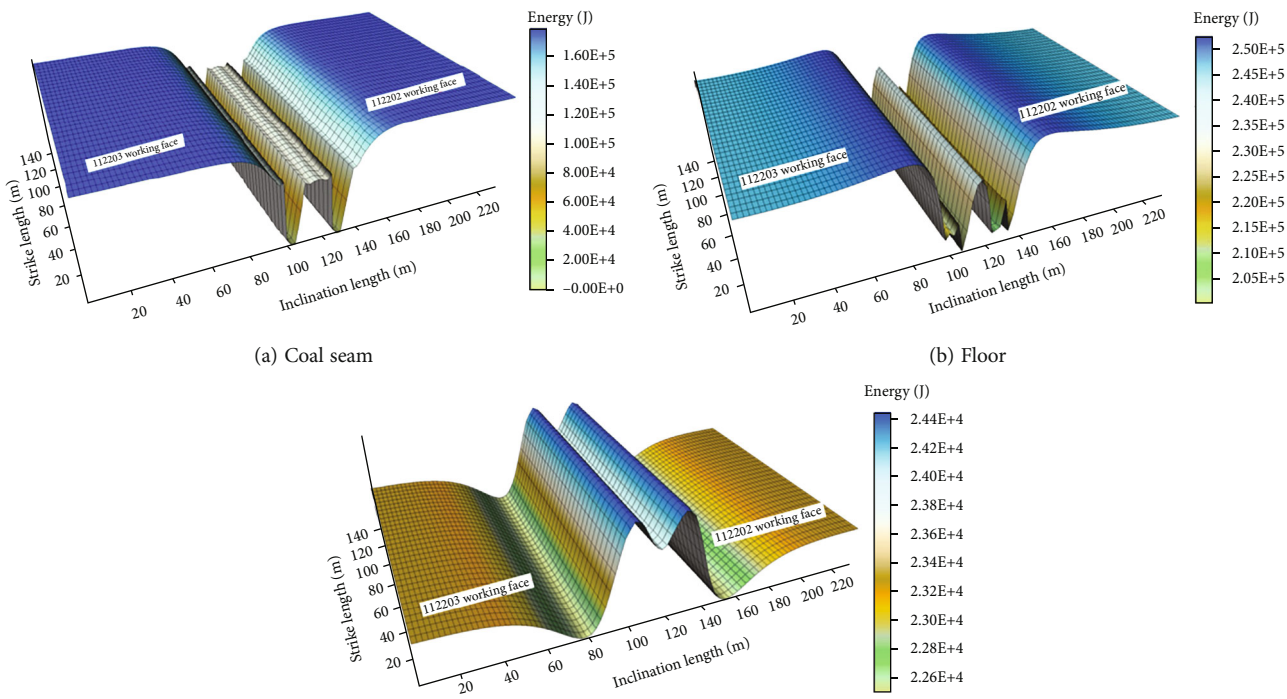

(a) Coal seam (b) Floor

(c) Roof

Figure 5: Energy distribution characteristics of the surrounding rock during double roadway excavation.

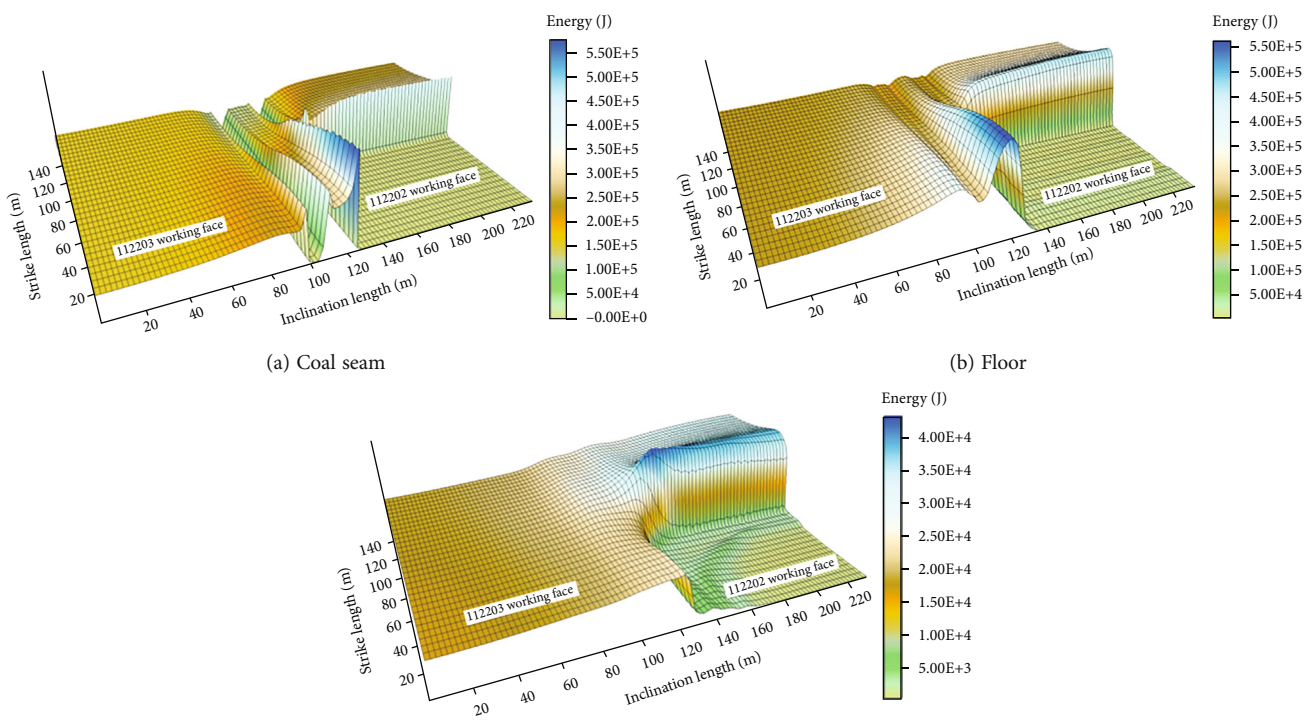

(a) Coal seam (b) Floor

(c) Roof

Figure 6: Energy distribution characteristics of the surrounding rock during primary mining.

an energy transfer path from the roof to the floor comes into being inside the coal pillar; the high static load energy is released through the goaf-side roadway and the leading segment of the roadway at the current working face, which leads to severe deformation failure in the roadway surrounding rock, thereby substantially impairing mine safety and production efficiency.

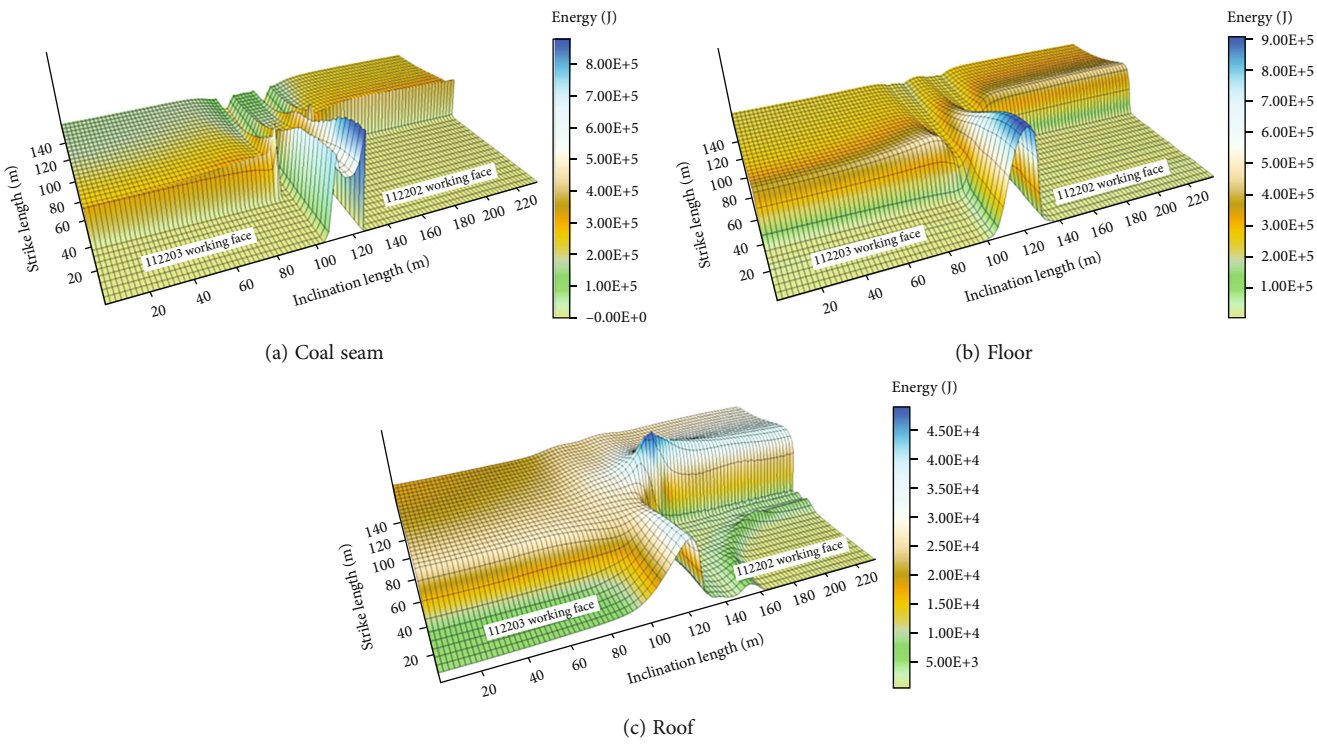

Figure 7: Energy distribution characteristics of the surrounding rock during secondary mining.

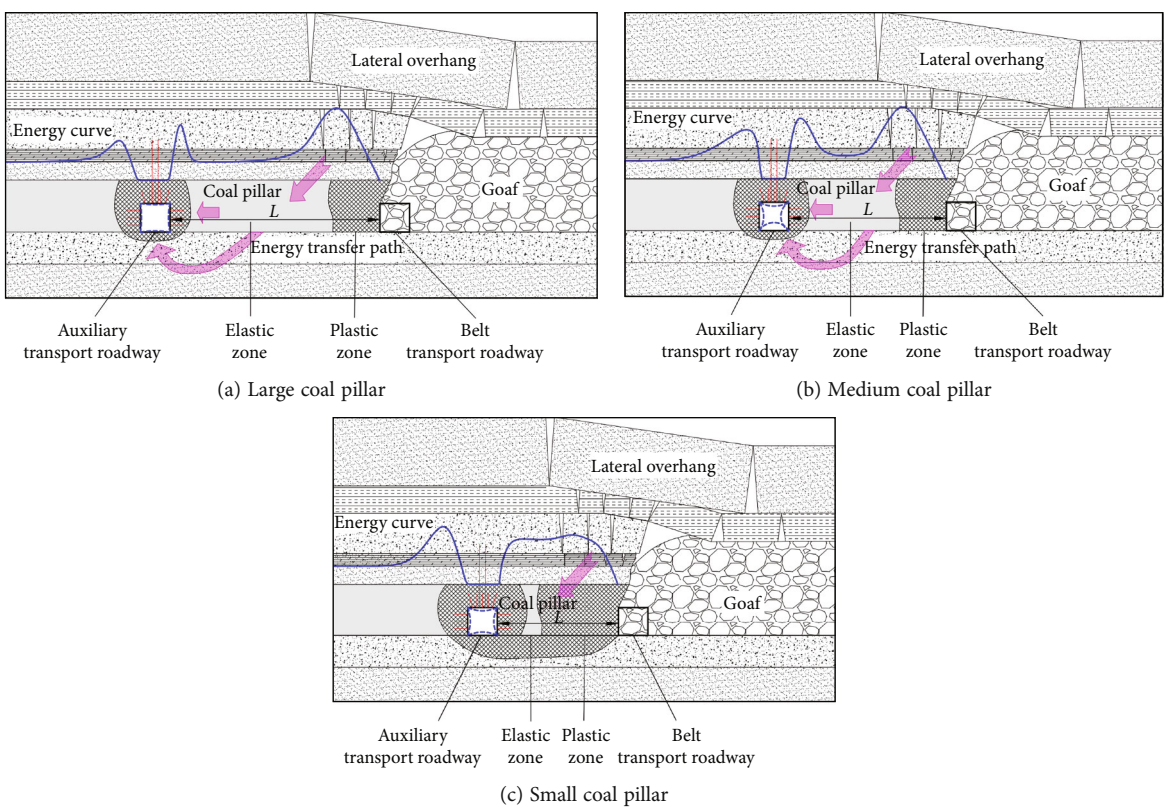

Figure 8: Deformation and failure characteristics of coal pillar roadways with different sizes.

3.2. Analysis of the Roadway Dynamic Pressure Manifestation Mechanism. According to the analysis presented in Section 3.1, the high static load energy in the roadway surrounding rock is principally concentrated near the coal pillar area. Since a coal pillar is a tie connecting the roof and floor, the rational setting of its size can affect the energy

transfer path in the surrounding rock and control the deformation in the roadway surrounding rock.

During coal seam mining, the overburden of the roof of the working face is broken, and a lateral overhang is formed in the roof of the goaf-side roadway. A coal pillar is squeezed by the rotary movement of the lateral overhang while transferring the energy load of the roof. As shown in Figure 8(a), when the coal pillar segment is large, the energy of the coal pillar shows a saddle-shaped distribution; the elastic zone in the middle of the coal pillar is wide, and the floor under the coal pillar also has an elastic zone. The high static load energy along the goaf-side coal pillar is transferred to the roadway along the goaf through the elastic zones of the coal pillar and the floor. Because of the considerable energy loss resulting from the long transfer path and because of the low energy in the middle of the coal pillar, the deformation of the roadway along the goaf is not prominent. When the coal pillar segment has an intermediate size, as shown in Figure 8(b), the static load energy transfer path becomes shorter, and the static load energy in the segment of the coal pillar further increases; the high static load energy is transferred to the roadway along the goaf via the elastic zones of the coal pillar and the floor, and the static load energy dissipation in the propagation path is lower, which may lead to severe rib spalling and floor heave in the roadway along the goaf. Where small coal pillars are used for roadway protection, the energy distribution in the coal pillar is convex; the elastic kernel in the middle of the coal pillar decreases, and the surrounding plastic zone increases. Moreover, plastic zones even develop in the coal pillar floor due to stress concentration, and the static load energy leads to failure along the transfer path in the coal pillar and the floor. Since the plastic zone of the surrounding rock can also absorb considerable static load energy during transfer, the deformation failure in the roadway along the goaf is less substantial, as shown in Figure 8(c). To guarantee the stability of the roadway surrounding rock along the goaf and reduce the extent of deformation and the number of reworks of the roadway surrounding rock, large or small coal pillars should be set up for roadway protection. Furthermore, the overhanging segment above the coal pillar can be subjected to roof cutting to reduce the static load energy agglomeration in the coal pillar.

4. Dynamic Pressure Roadway Stability Control

Because of the unreasonable setting of coal pillar size and the presence of lateral overhang in the roadway along the goaf, the roadway surrounding rock undergoes severe deformation failure under the action of multiple mining operations, leading to considerable dynamic pressure manifestation; hence, the roadway surrounding rock stability can be controlled by optimizing the segment coal pillar size and fracturing roof cutting.

4.1. Coal Pillar Size Optimization. For the optimization, the load estimation method and the elastic kernel theory calculation method were used to study the width settings of segment coal pillars in the roadway [27, 28]; numerical simulation was performed to analyse the distribution of the plastic zones of coal pillars of different widths during driving and mining operations to determine rational size settings for the coal pillars.

4.1.1. Load Estimation. The load per unit width of the segment coal pillar is

$$\sigma = \frac{\rho g\left[(B+D)\cdot H - 0.25D^2 \cot\delta\right]}{B}, \tag{1}$$

where B is the width of the segment coal pillar, m; D is the goaf width, which is 350 m; δ is the natural caving angle of the rock stratum, which is 43°; ρ is the average density of the rock formation, which is 2.5 t/m^3; and H is the buried depth of the roadway, which is 321.06 m.

The load limit of a coal pillar is as follows:

$$R = R_{c2}\left(0.64 + 0.36\frac{B}{h}\right), \tag{2}$$

where R is the load limit of the coal pillar; R_{c2} is the uniaxial compressive strength of the coal mass, which is 18.2 MPa; and h is the height of the segment coal pillar, which is 4.4 m.

To keep the coal pillars stable, the average load to which they are subjected should not exceed their load limit; that is

$$\sigma \le R. \tag{3}$$

Therefore, the rational width of the segment coal pillar should not be less than 33.7 m.

4.1.2. Elastic Kernel Theory Calculation. The width of the yield zone of a coal pillar is

$$W_1 = \frac{hd}{2\tan\theta}\left[\ln\left(\frac{C+\sigma_{zl}\tan\theta}{C+(p_x/\beta)\tan\theta}\right)^{\beta} + \tan^2\theta\right], \tag{4}$$

where p_x is the lateral restriction of the coal pillar, which is 0.1 MPa; d is the mining disturbance coefficient, which is 1.5-3.0; β is the lateral pressure coefficient at the interface between the yield zone and the elastic kernel zone, which is 0.4; σ_{zl} is the pillar strength, which is 52.5 MPa; C is the coal pillar cohesion, which is 0.61 MPa; and θ is the internal friction angle of the coal pillar, which is 38.48°.

The width of the plastic zone of the coal pillar is

$$W_2 = r\left\{\left[\frac{\gamma H\tan\theta + C}{p\tan\theta + C}(1-\sin\theta)\right]^{1-\sin\theta/2\sin\theta} - 1\right\}, \tag{5}$$

where γ is the average bulk density of the coal mass, which is 13.2 kg/m^3; p is the support resistance, which is 0.16 MPa; and r is the equivalent radius of the roadway, which is 2.6 m.

The width of the coal pillar is

$$B = K(W_1 + W_2), \tag{6}$$

where K is the safety factor, which is 1.3.

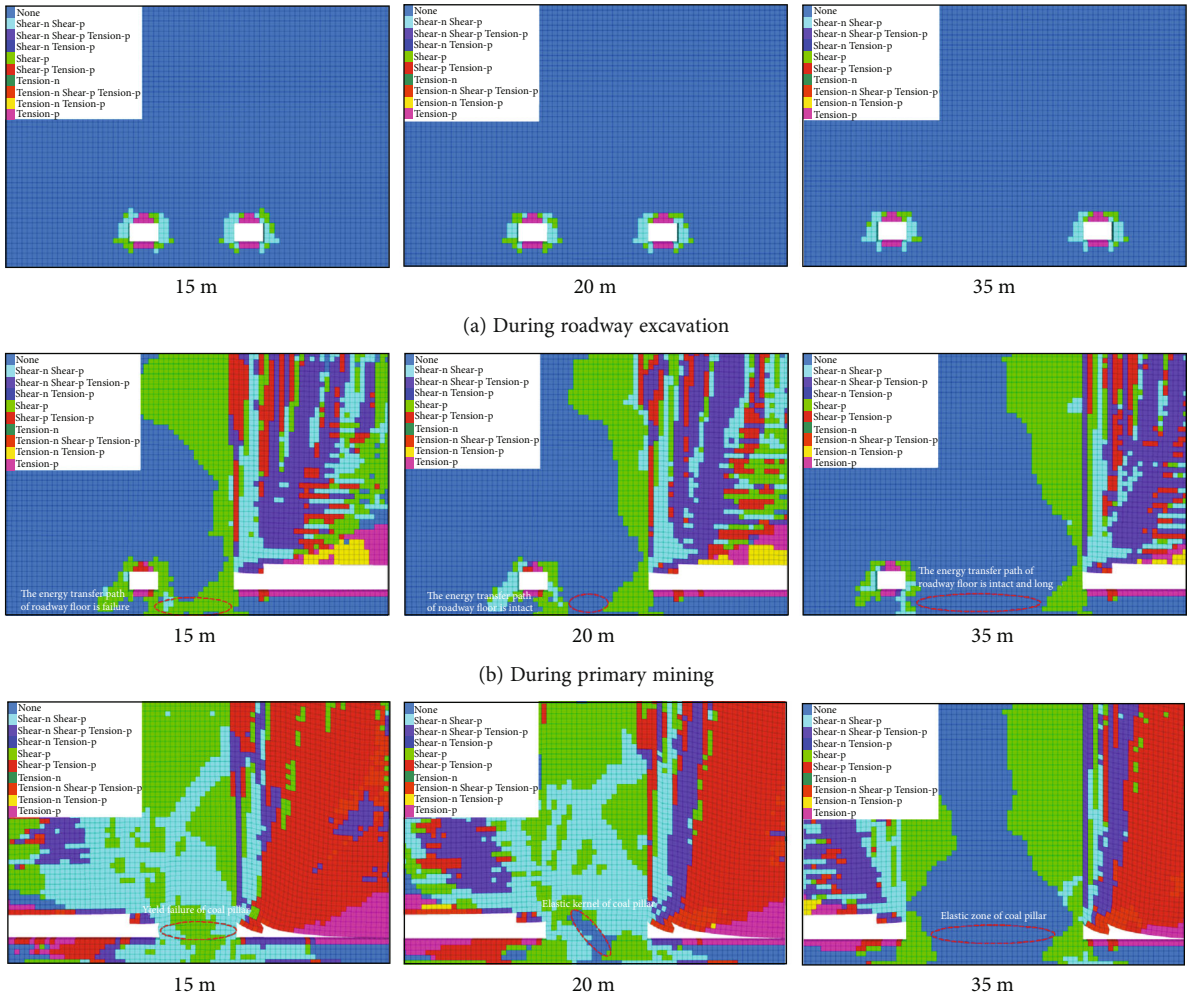

15 m 20 m 35 m

(a) During roadway excavation

15 m 20 m 35 m

(b) During primary mining

15 m 20 m 35 m

(c) During secondary mining

Figure 9: Distribution characteristics of the plastic zone of the roadway surrounding rock in different mining stages.

Therefore, the rational width of the segment coal pillar is 15.35 m.

These results suggest that where large coal pillars for roadway protection are arranged for the working face, the coal pillar size should not be smaller than 33.7 m and is recommended to be 35 m; where small coal pillars for roadway protection are arranged for the working face, the coal pillar size should not exceed 15.35 m and is recommended to be 15 m. The segment coal pillar size for the current working face of the mine is 20 m, which is greater than that for small pillars and smaller than that for large pillars, that is, the coal pillars are medium-sized, where the elastic kernels easily form energy transfer channels. Thus, dynamic pressure manifestations such as floor heave and rib spalling occur frequently in the roadways.

On the basis of the theoretical calculation and the current coal pillar size, numerical software was used to simulate the distributions of the plastic zone during driving, primary mining, and secondary mining in coal pillar widths of 15, 20, and 35 m, thereby analysing the integrity of the energy transfer channel inside the coal pillars that are shown in Figure 9.

Coal pillars are slightly affected by the driving stress during double roadway excavation driving. The plastic zones are 2 m for coal pillars of various widths in the roadway roof and sides and 1 m in the floor. During primary mining, the development depth of the plastic zone on both sides of the 15 m coal pillar is 9 m; a 6 m elastic kernel remains in the middle of the coal pillar, and the pillar and floor plastic zones develop in this segment, which destroys the energy transfer path in the roadway surrounding rock. In the following face stoping operation, floor heave and rib spalling in the roadways are relieved. An 11 m elastic kernel occurs in the middle of the 20 m coal pillar, and the elastic energy transfer channels of the floor are well preserved to maintain good transfer behaviour, which may cause severe deformation failure in the roadway surrounding rock. A 27 m elastic kernel occurs in the middle of the 35 m coal pillar, despite the good integrity of the surrounding rock at the energy transfer channels, and the deformation failure in the roadway along the goaf may weaken to some extent due to the long energy transfer channels. During secondary mining, the 15 m coal pillar behind the goaf fails with perfect plastic

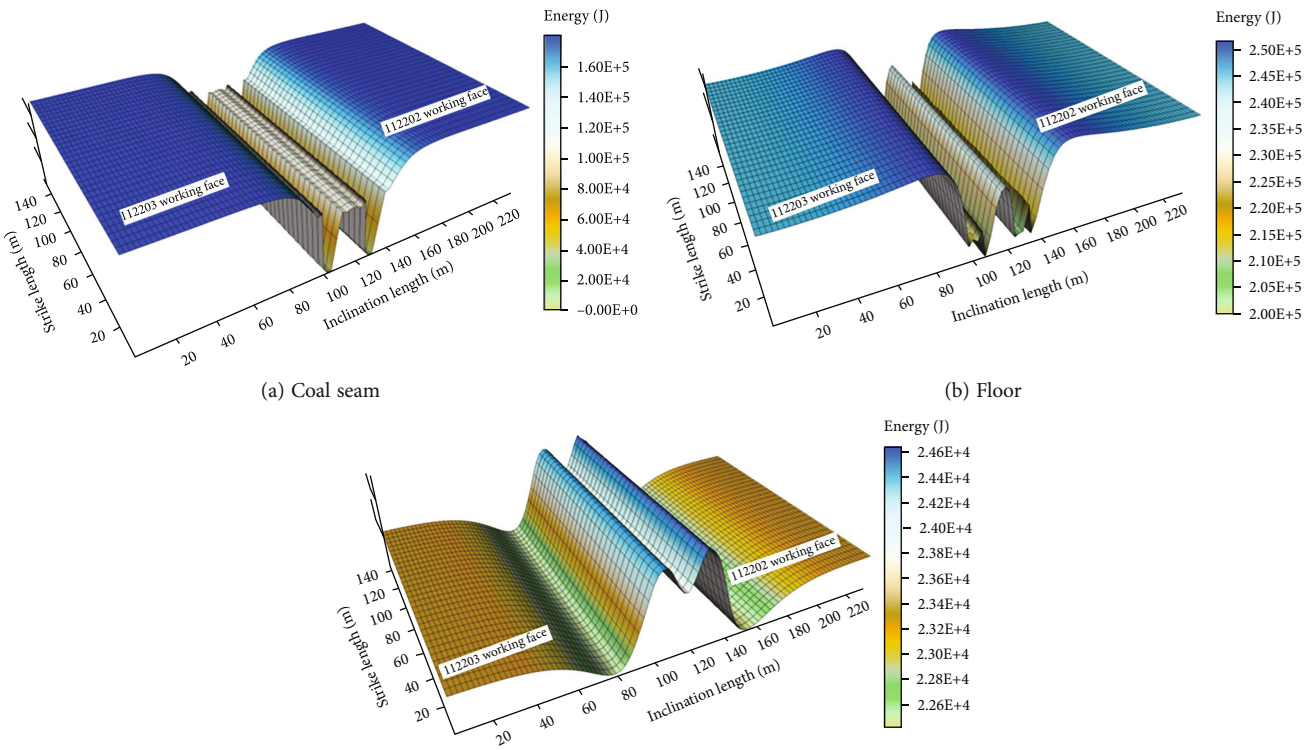

(a) Coal seam (b) Floor

(c) Roof

Figure 10: Energy distribution characteristics of the surrounding rock in hydraulic fracturing roof cutting of the roadway during double roadway excavation.

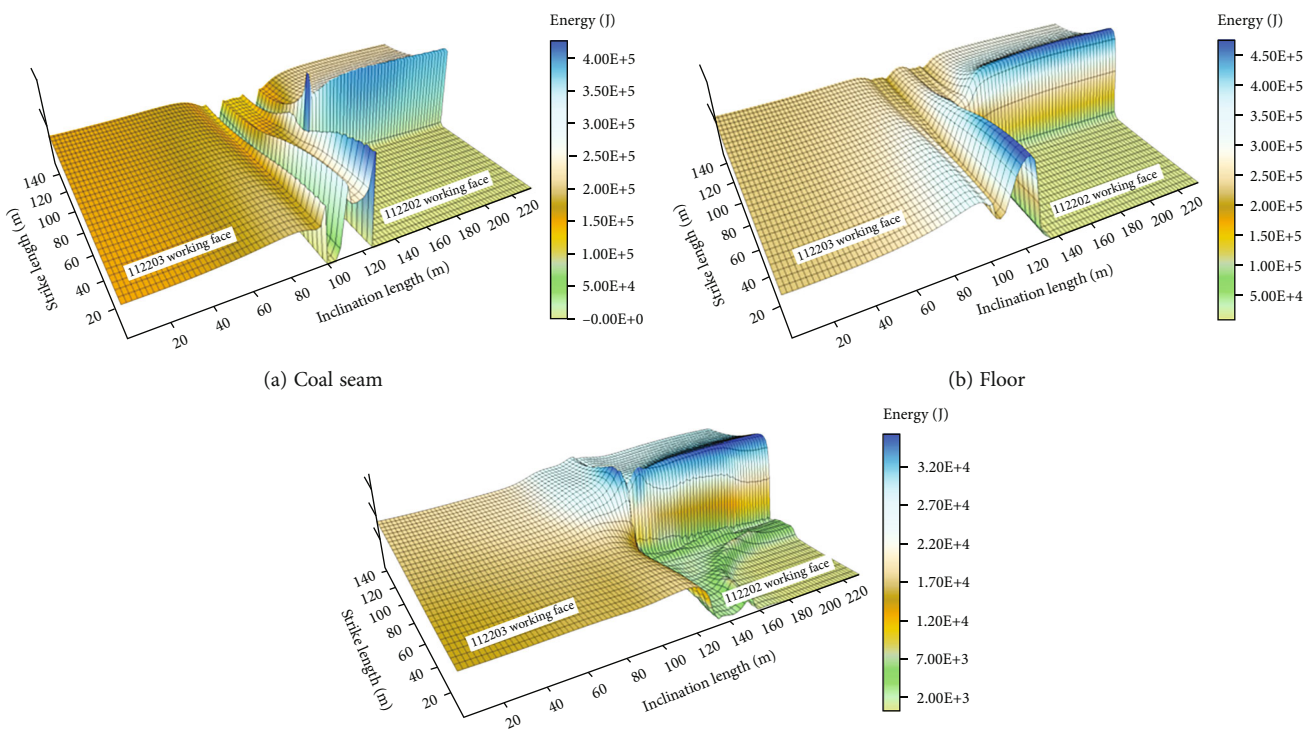

(a) Coal seam (b) Floor

(c) Roof

Figure 11: Energy distribution characteristics of the surrounding rock in hydraulic fracturing roof cutting of the roadway during primary mining.

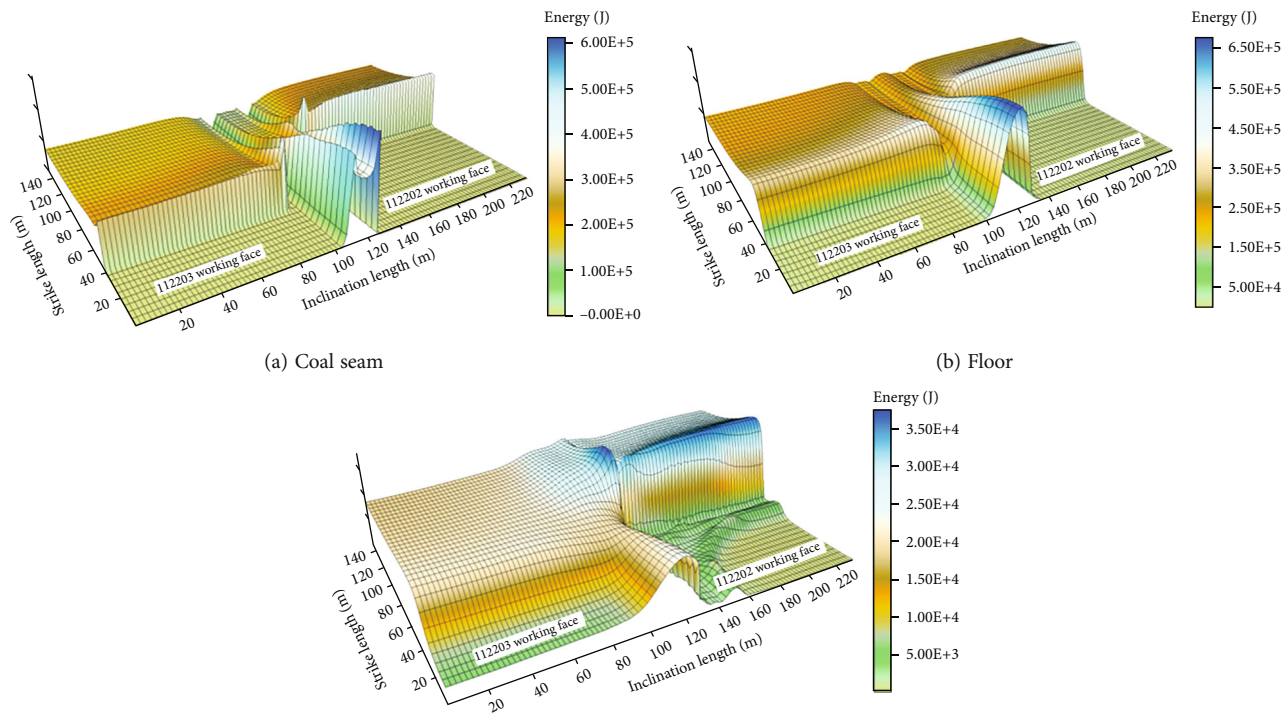

(a) Coal seam (b) Floor

(c) Roof

Figure 12: Energy distribution characteristics of the surrounding rocks in hydraulic fracturing roof cutting of the roadway during secondary mining.

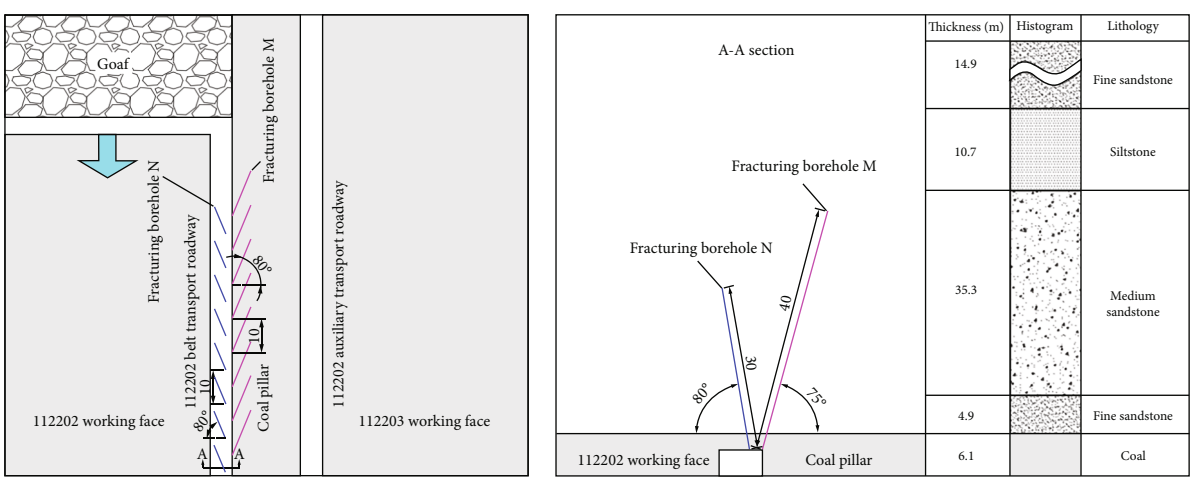

(a) Top view (b) A-A cross section

Figure 13: Layout plan of hydraulic fracturing boreholes.

yield; thus, it is not suitable for transferring the roof energy in the goaf, and as a result, the leading segment of roadway along the goaf will be well preserved. A 4 m elastic kernel is still in the middle of the 20 m coal pillar; the high static load energy and good transfer of the goaf roof energy in this area will lead to gross deformation in the leading segment of the roadway along the goaf. There is a 24 m elastic kernel in the middle of the 35 m coal pillar, and the coal pillar therefore exhibits good stability and low static load energy; the resulting poor transfer of roof energy towards the leading zone enables the roadway stability to be well preserved. Using the 15 m coal pillars for roadway protection destroys the energy transfer path in the coal pillars. Where 35 m coal pillars are used for roadway protection, the wide elastic zone in the middle of the coal pillar, the insignificant static load energy agglomeration, the long energy transfer path in the pillars, and the high loss during energy transfer lead to high stability in the roadway surrounding rock.

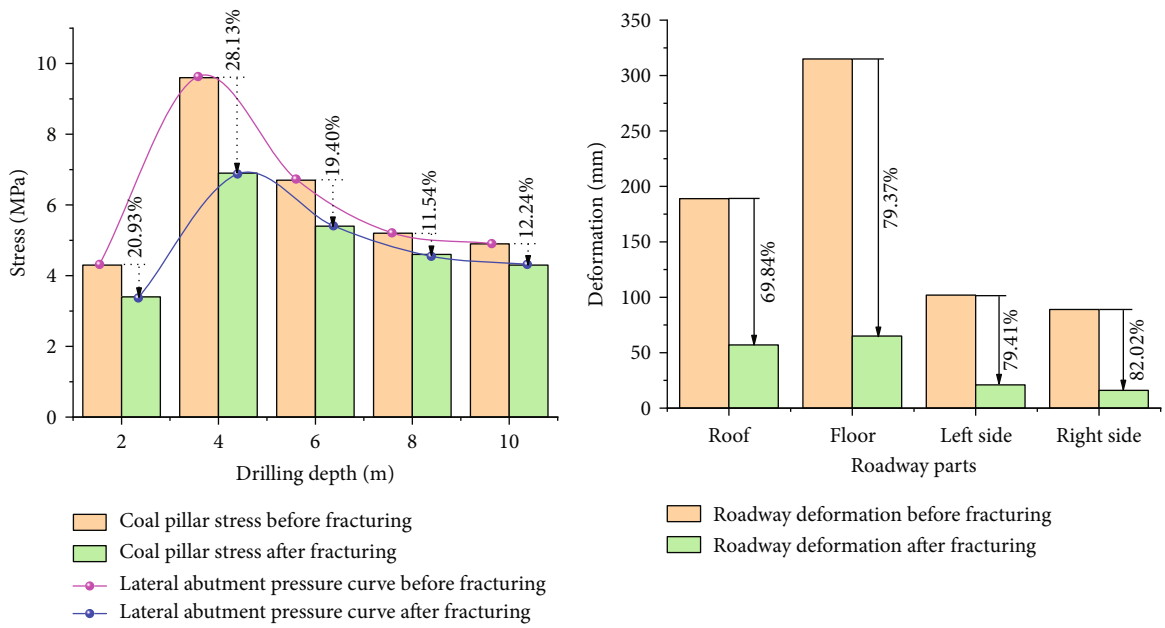

(a) Coal pillar stress (b) Roadway deformation

Figure 14: Stress and deformation characteristics of the roadway surrounding rock before and after hydraulic fracturing.

(a) 50 m in front of working face 112202 (b) 200 m behind working face 112202

Figure 15: Control effect of hydraulic fracturing of the surrounding rock of auxiliary transport roadway 112202.

4.2. Roof Cutting by Hydraulic Fracturing. Because of the presence of a thick hard sandstone roof in the overlying strata of the working face, the pillar-side roof behind the goaf develops a cantilever beam structure after push mining at the working face. The bending and subsidence of the cantilever beam lead to energy accumulation inside the coal pillar, which induces rib spalling and floor heave in the roadway surrounding rock. Hence, hydraulic fracturing can be used to cut off the lateral overhang at the working face to alleviate the static load energy agglomeration in the coal pillar. The collapsed rock formations fill the goaf over time, thereby weakening the static load source and improving the characteristics of the energy distribution in the coal pillar [29–31]. With the existing 20 m coal pillar as an example, according to the numerical simulation of roof cutting for pressure relief, the roof-cutting line is located on the side of belt transport roadway 112202 against the coal pillar, and the roof-cutting height is 40 m, which helps avoid the thick hard sandstone roof forming an overhang on the coal pillar side.

As shown in Figure 10, the thick hard sandstone roof is roof-cut after double roadway excavation driving; since the working face is unaffected by the mining disturbance, hydraulic fracturing for roof cutting creates little disturbance in the energy distribution characteristics of the roadway surrounding rock, while the energy values of the coal seam and roof and floor do not change appreciably compared with those before roof cutting.

As shown in Figure 11, because of the stoping at working face 112202, the roadway surrounding rock is subjected to

the effects of a primary mining operation. Since the roof of the working face is roof-cut, the overhang behind the goaf can be caved over time to fill the goaf; hence, the energy values in the coal pillar segments and the roof and floor of the working face are substantially lower than before roof cutting. The energy at the coal pillar side of belt transport roadway 112202 in the goaf behind the working face is 4.28×10^5 J, the energy at the coal pillar side of auxiliary transport roadway 112202 is 3.49×10^5 J, and the intermediate energy of the coal pillars is 2.37×10^5 J, indicating a 17.71-26.33% decrease from before roof cutting. The energy in the floor of the coal pillars is 4.74×10^5 J, a 15.66% decrease from before roof cutting. The energy accumulation zone in the roof shifts from above the coal seam to near the cutting line of the segment coal pillar, where the energy is 3.64×10^4 J, a decrease of 14.35% from before fracturing. The energy in the coal mass of the end area of the working face is 4.49×10^5 J, an increase of 6.40% from before fracturing, which demonstrates that the intensification of roof activity in the advanced mining-affected zone leads to an increase in the energy of the coal mass in the end area of the working face after fracturing for roof cutting; hence, the roof support strength should be enhanced in the end area of the working face with roof cuts.

As shown in Figure 12, the stoping at working face 112203 causes the roadway surrounding rock to be affected by secondary mining; the energy in the segment coal pillar and the roof and floor of the working face after fracturing for roof cutting decreases from before roof cutting. The energy in the coal pillar at the goaf side of working face 112202 is 6.21×10^5 J, the energy in the coal pillar at the goaf side of working face 112203 is 5.62×10^5 J, and the intermediate energy of the coal pillars is 3.73×10^5 J, a 28.41-29.31% decrease from before roof cutting; the energy in the floor of the coal pillars is 6.79×10^5 J, a decrease of 26.12% from before roof cutting; the energy accumulation zone of the roof remains near the roof-cutting line of the coal pillar, where the energy is 3.71×10^4 J, a 21.57% decrease from before fracturing; and the energy in the coal mass in the end area of the return air roadway is 5.81×10^5 J, a 0.69% increase from before fracturing. The energy in the coal mass at the working face end does not change appreciably after fracturing for roof cutting.

A comprehensive comparison suggests that the energy variations in the surrounding rock are not substantial before the mining effect on the working face and after roadway fracturing for roof cutting. During primary mining, the energy near the roof cut of the roadway surrounding rock may decrease by 14.35-26.33%. During secondary mining, the energy near the roof cut of the roadway surrounding rock may decrease by 21.57-29.31%. After roof cutting, the energy decreases, and the stability of the roadway surrounding rock increases during primary and secondary mining operations.

5. Engineering Applications

Because the production system was established at working face 112202, the pillar size cannot be adjusted; hence, hydraulic fracturing is performed for roof cutting at belt transport roadway 112202 to cut off the lateral overhang of the working face, thereby alleviating the manifestation of the dynamic pressure in the roadway surrounding rock, suppressing the deformation of the surrounding rock in the mining roadway, and ensuring safe production at the working face.

5.1. Scheme Design. Fracturing holes are arranged at the gateway 500 m from the leading working face; fracturing holes M are arranged axially along the gateway with spacings of 10 m, depths of 40 m, axial angles to the roadway of 10°, and dip angles of 75°; fracturing holes N are arranged axially along the roadway 1.0 m away from the coal pillar with spacings of 10 m, depths of 30 m, axial angles to the roadway of 10°, and dip angles of 80°. The sealing length of the hydraulic fracturing borehole is 10 m, and the fracturing pressure is 25-30 MPa. The hydraulic fracturing scheme design is shown in Figure 13.

5.2. Effect Analysis. The effect of controlling the surrounding rock through roof cutting for pressure relief was analysed by monitoring the stress distribution characteristics in the coal pillar at auxiliary transport roadway 112202 200 m behind the goaf and the deformation of the roadway surrounding rock before and after fracturing.

Figure 14 shows that after hydraulic fracturing for roof cutting, the internal stress of the coal pillar decreased by 11.54-28.13%, and the deformations of the roadway surrounding rock decreased by 69.84-82.02%. Hydraulic fracturing substantially improved the stability of the roadway surrounding rock, and the floor heave and rib spalling were weakened in the roadway surrounding rock, which guarantees safe stoping at the working face. The control effect of fracturing the surrounding rock of auxiliary transport roadway 112202 is shown in Figure 15.

6. Conclusion

(1) The causes of the failures in roadway surrounding rock with large mining heights and intense mining have been analysed. The surrounding rock failures in mining roadways are principally affected by factors such as roadway layout orientation, mining intensity, and dynamic load disturbances caused by roof breakage

(2) The energy distribution characteristics during roadway driving and mining operations were studied to determine the mechanism of surrounding rock deformation failures in dynamic pressure roadways. Slight energy accumulation occurs near the surrounding rock during driving operations. Energy accumulation increases near the roadway surrounding rock during primary and secondary mining, and the elastic energy near the surrounding rock during secondary mining increases by 49.57-80.90% compared to that during primary mining. Since the coal pillar is a "bridge" connecting the roof and floor, a rational setting of its dimensions may affect the energy transfer path in the roadway surrounding

rock. Using small or large coal pillars for roadway protection can increase the loss of energy in the transfer path to provide effective control of surrounding rock deformations

(3) A surrounding rock stability control technique and related measures are proposed for dynamic pressure roadways. Segment coal pillar size optimization and fracturing for roof cutting help control roadway surrounding rock deformation; small 15 m coal pillars and large 35 m coal pillars for roadway protection may destroy the energy transfer path or increase the elastic energy loss in the transfer path; with roof cutting for pressure relief, the elastic energy near the roadway surrounding rock decreases by 14.35-26.33% and 21.57-29.31% during primary and secondary mining, respectively. With field roof cutting for pressure relief, the stress in the roadway surrounding rock is reduced by 11.54-28.13%, and the deformation decreases by 69.84-82.02% during primary and secondary mining, respectively, ensuring the safe and efficient stoping operations at the working face

Data Availability

Some of the data used to support the findings of this study are included within the article, and the other data are available from the corresponding author upon request.

Conflicts of Interest

The authors declare no conflicts of interest.

Acknowledgments

This work is supported by the National Natural Science Foundation Project of China (51564044) and the China Scholarship Council (CSC No. 202106420060).

References

[1] P. Malkowski, L. Ostrowski, and J. Stasica, "Modeling of floor heave in underground roadways in dry and waterlogged conditions," *Energies*, vol. 15, no. 12, 27 pages, 2022.

[2] G. Y. Yu, J. Wang, J. Hu et al., "Innovative control technique for the floor heave in goaf-side entry retaining based on pressure relief by roof cutting," *Mathematical Problems in Engineering*, vol. 2021, Article ID 7163598, 17 pages, 2021.

[3] S. Z. Zhang, G. W. Fan, L. Chai et al., "Disaster control of roof falling in deep coal mine roadway subjected to high abutment pressure," *Geofluids*, vol. 2021, Article ID 8875249, 17 pages, 2021.

[4] D. Xu, M. S. Gao, Y. L. He, and X. Yu, "A study on the mechanical properties and bursting liability of coal-rock composites with seam partings," *Advance in Civil Engineering*, vol. 2021, article 9953241, 13 pages, 2021.

[5] X. P. Lai, H. Xu, P. Shan, Y. Kang, Z. Wang, and X. Wu, "Research on mechanism and control of floor heave of mining-influenced roadway in top coal caving working face," *Energies*, vol. 13, no. 2, 14 pages, 2020.

[6] W. L. Zhai, F. L. He, X. H. Xu, K. Lv, L. Li, and J. Y. Song, "Floor heave mechanism in water-rich soft rock roadways and a DS-IBA control approach," *Geomatics Natural Hazards & Risk*, vol. 13, no. 1, pp. 2107–2123, 2022.

[7] A. Chen, X. B. Li, X. S. Liu, Y. L. Tan, K. Xu, and H. L. Wang, ""Relief-retaining" control technology of floor heave in mining roadway with soft rock: a case study," *Advance in Civil Engineering*, vol. 2021, article 1455052, 13 pages, 2021.

[8] X. M. Sun, F. Chen, M. C. He, W. L. Gong, H. C. Xu, and H. Lu, "Physical modeling of floor heave for the deep-buried roadway excavated in ten degree inclined strata using infrared thermal imaging technology," *Tunnelling and Underground Space Technology*, vol. 63, pp. 228–243, 2017.

[9] S. Mo, H. L. Ramandi, J. Oh et al., "A new coal mine floor rating system and its application to assess the potential of floor heave," *International Journal of Rock Mechanics And Mining Sciences*, vol. 128, article 104241, 2020.

[10] S. Mo, K. Tutuk, and S. Saydam, "Management of floor heave at Bulga underground operations - a case study," *International Journal of Mining Science and Technology*, vol. 29, no. 1, pp. 73–78, 2019.

[11] R. Peng, X. R. Meng, G. M. Zhao, Y. M. Li, and J. M. Zhu, "Correction: experimental research on the structural instability mechanism and the effect of multi-echelon support of deep roadways in a kilometre-deep well," *PLoS One*, vol. 13, no. 9, article e0204059, 24 pages, 2018.

[12] X. Y. Xiong, J. Dai, Y. Ouyang, and P. Shen, "Experimental analysis of control technology and deformation failure mechanism of inclined coal seam roadway using non-contact DIC technique," *Scientific Reports*, vol. 11, no. 1, article 20930, 23 pages, 2021.

[13] J. X. Liu, J. Wu, Y. Dong et al., "Research on control mechanism of surrounding rock of deep gob-side entry retaining," *Geofluids*, vol. 2021, Article ID 2729122, 10 pages, 2021.

[14] S. B. Li, L. Wang, C. Zhu, and Q. Ren, "Research on mechanism and control technology of rib spalling in soft coal seam of deep coal mine," *Advances in Materials Science and Engineering*, vol. 2021, Article ID 2833210, 9 pages, 2021.

[15] G. J. Zhang, Q. S. Li, Y. Zhang, and F. Du, "Failure characteristics of roof in working face end based on stress evolution of goaf," *Geomechanics and Geophysics for Geo-Energy and Geo-Resources*, vol. 7, no. 3, 22 pages, 2021.

[16] E. Wang, G. B. Chen, X. J. Yang, G. F. Zhang, and W. B. Guo, "Study on the failure mechanism for coal roadway stability in jointed rock mass due to the excavation unloading effect," *Energies*, vol. 13, no. 10, 19 pages, 2020.

[17] B. T. Shen and N. Barton, "Rock fracturing mechanisms around underground openings," *Geomechanics and Engineering*, vol. 16, no. 1, pp. 35–47, 2018.

[18] J. C. Feng, S. Yin, Z. Cheng et al., "Deformation and failure mechanism of surrounding rock in mining-influenced roadway and the control technology," *Shock and Vibration*, vol. 2021, Article ID 5588314, 14 pages, 2021.

[19] H. W. Wang, S. Xue, Y. Jiang, D. Deng, S. Shi, and D. Zhang, "Field investigation of a roof fall accident and large roadway deformation under geologically complex conditions in an underground coal mine," *Rock Mechanics and Rock Engineering*, vol. 51, no. 6, pp. 1863–1883, 2018.

[20] B. Jiang, Q. Wang, L. Gao et al., "Limit analysis of roof falling in roadway with water-rich surrounding rock," *Geotechnical*

and Geological Engineering, vol. 35, no. 5, pp. 2361–2369, 2017.

[21] H. J. Dong, J. Zhang, and F. Zhang, "Study on deformation and supporting measures of mining roadway with compound roof," *Geotechnical and Geological Engineering*, vol. 40, no. 3, pp. 1449–1462, 2022.

[22] X. C. Kang, D. Guo, and Z. Lu, "Mechanism of roadway floor heave controlled by floor corner pile in deep roadway under high horizontal stress," *Advances in Civil Engineering*, vol. 2021, Article ID 6669233, 10 pages, 2021.

[23] R. H. Cao, P. Cao, and H. Lin, "A kind of control technology for squeezing failure in deep roadways: a case study," *Geomatics Natural Hazards & Risk*, vol. 8, no. 2, pp. 1715–1729, 2017.

[24] H. Yan, X. J. Deng, K. Fang, S. Guo, and W. K. Li, "Roof catastrophe mechanism of roadways with extra-thick coal seam and its controlling countermeasures," *Disaster Advances*, vol. 6, pp. 236–243, 2013.

[25] C. L. Zhu, J. Zhang, M. Li, Z. He, Y. Wang, and Y. Lan, "Effect mechanism of strata breakage evolution on stope deformation in extra- thick coal seams," *Alexandria Engineering Journal*, vol. 61, no. 6, pp. 5003–5020, 2022.

[26] X. H. Xu, F. He, X. Li, and W. He, "Research on mechanism and control of asymmetric deformation of gob side coal roadway with fully mechanized caving mining," *Engineering Failure Analysis*, vol. 120, article 105097, 12 pages, 2021.

[27] D. Z. Kong, Z. H. Wang, X. M. Li, Y. L. Wang, and C. Wang, "Study of reasonable width of full-mechanized top-coal caving with large mining height," *Rock and Soil Mechanics*, vol. 35, no. 2, pp. 460-461, 2014.

[28] B. Wang, F. X. Jiang, S. T. Zhu et al., "Mechanism and prevention of rock burst induced by segment pillars in the deep mining areas of Shaanxi-Inner Mongolia adjacent regions," *Journal of Mining & Safety Engineering*, vol. 37, no. 3, pp. 505–513, 2020.

[29] F. T. Zhang, X. Y. Wang, J. B. Bai, W. D. Wu, B. W. Wu, and G. H. Wang, "Fixed-length roof cutting with vertical hydraulic fracture based on the stress shadow effect: a case study," *International Journal of Mining Science and Technology*, vol. 32, no. 2, pp. 295–308, 2022.

[30] J. W. Liu, C. Y. Liu, Q. L. Yao, and G. Y. Si, "The position of hydraulic fracturing to initiate vertical fractures in hard hanging roof for stress relief," *International Journal of Rock Mechanics and Mining Sciences*, vol. 132, 13 pages, 2020.

[31] B. X. Huang, Q. Y. Cheng, X. L. Zhao, W. C. Xue, and M. Scoble, "Using hydraulic fracturing to control caving of the hanging roof during the initial mining stages in a longwall coal mine: a case study," *Arabian Journal of Geosciences*, vol. 11, no. 20, 16 pages, 2018.